Kelvin and Rossby gravity wave packets in the lower stratosphere of some high-top CMIP5 models

F. Lott[1], S. Denvil[2], N. Butchart[3], C. Cagnazzo[4], M. A. Giorgetta[5], S. C. Hardiman[3], E. Manzini[5], T. Krismer[5], J-P Duvel[1], P. Maury[1], J. F. Scinocca[6], S. Watanabe[7], and S. Yukimoto[9]

Abstract.

We analyse the stratospheric Kelvin and Rossby-gravity wave packets with periods of a few days in nine high-top (i.e. with stratosphere) models of the fifth Coupled Model Intercomparison Project (CMIP5). These models simulate realistic aspects of these waves, and represent them better than the tropospheric convectively coupled waves analyzed in previous studies.

There is nevertheless a large spread among the models, and those with a Quasi-Biennial Oscillation (QBO) produce larger amplitude waves than the models without a QBO. For the Rossby-gravity waves this is explained by the fact that models without a QBO never have positive zonal mean zonal winds in the lower stratosphere, a situation that is favorable to the propagation of Rossby-gravity waves. For the Kelvin waves, larger amplitudes in the presence of a QBO is counter intuitive because Kelvin waves are expected to have larger amplitude when the zonal mean zonal wind is negative, and this is always satisfied in models without a QBO. We attribute the larger amplitude to the fact that models tuned to have a QBO require finer vertical resolution in the stratosphere.

We also find that models with large precipitation variability tend to produce larger amplitude waves. However, the effect is not as pronounced as was found in previous studies. In fact, even models with weak precipitation variability still have quite realistic stratospheric waves, indicating either that (i) other sources can be significant or that (ii) the dynamical filtering mitigates the differences in the sources between models.

1. Introduction

Kelvin and Rossby gravity wave packets with periods of a few days dominate the day-to-day variability in the lower equatorial stratosphere. Such waves were first observed by Wallace and Kousky (1968) and Yanai and Maruyama (1966), and many studies have now documented their presence in vertical soundings or ground-based observations (Tsuda et al. 1994, Sassi et al. 2003, Fujiwara et al. 2003), and using ultralong-duration balloons (Vial et al. 2001, Hertzog and Vial 2001). These direct observations are today complemented by observations from meteorological satellites which provide a global description of the stratospheric equatorial waves (SEWs; Salby et al. 1984, Randel and Gille 1991, Mote et al. 2002, Mote and Dunkerton 2004, Alexander and Ortland 2010) and some of these satellite observations are now routinely assimilated in global models. This makes the SEWs quite well represented in meteorological analysis but significant errors still exist (for the ECMWF analyses see Ern et al. 2008). These errors likely explain that the different reanalysis available today present a large spread in their representation of the SEWs (at the tropopause level see Fujiwara et al. 2012). As an illustration, the under estimation of wave activity in the ECMWF analysis found by Ern et al. (2008) that is mainly related to the Rossby gravity waves, is still present in ERA-Interim (Maury et al. 2013).

It is generally accepted that SEWs are largely forced by tropospheric convection (e.g., Holton 1972, Manzini and Hamilton 1993), and are partly related to the tropospheric convectively coupled equatorial waves (CCEWs) described by Wheeler et al. (2000) which travel coherently with convective centers in the troposphere (Hendon and Wheeler 2008). A clear example is given in Maury et al. (2013) where it is shown that SEWs are often present above CCEWs. Nevertheless, Hendon and Wheeler (2008) also show that the coherencies between equatorial waves and convection rapidly decrease with altitude because the CCEWs are rather slow. As a result their periods correspond to short vertical wavelength in the stratosphere where they dissipate rapidly. More recently, Alexander and Ortland (2010) have shown that the temporal variations of Kelvin wave activity in the tropical tropopause layer (TTL) and the stratosphere follows changes in propagation conditions (i.e., background winds and stability) rather than changes in Kelvin wave activity in convection. This dynamical filtering is also clearly apparent in Flannaghan and Fueglistaler (2013) which shows that the global wind fields

[1]Laboratoire de Météorologie Dynamique, Ecole Normale Supérieure, 24 rue Lhomond, 75231 Paris Cedex 05, France
[2]IPSL, Université Pierre et Marie Curie, 4 place Jussieu, 75252 Paris Cedex 05, France
[3]Met Office, FitzRoy Rd, Exeter Devon EX1 3PB, United Kingdom
[4]ISAC-CNR, Via Fosso del Cavaliere 100 00133 - Roma, Italy
[5]Max-Planck-Institut fur Meteorologie, Bundesstrasse 53, 20146 Hamburg, Germany
[6]CCCMA, University of Victoria, 3800 Finnerty Road, Victoria BC V8P 5C2, Canada
[7]Japan Agency for Marine-Earth Science and Technology 3173-25 Syowa-machi, Kanazawa-ku Yokohama Kanagawa 236-0001 Japan
[8]Climate Research Department, Meteorological Research Institute 1-1 Nagamine, Tsukuba 305-0052, Japan

0148-0227/14/$9.00

induce a longitudinal mismatch between enhanced Kelvin wave activity in the TTL and in the Kelvin wave activity in tropospheric convection. Under favorable background flow conditions, this dynamical filtering can induce large SEWs even when the convection is not organized by CCEWs (Garcia and Salby 1987) or when the sources are not the equatorial convection (Maury and Lott 2013).

A large number of studies have analysed the extent to which middle atmosphere General Circulation Models (GCMs) simulate SEWs (Boville and Randel 1992, Manzini and Hamilton 1993, Amodei et al. 2001). They show that GCMs can produce SEWs but that their amplitude is very sensitive to the convective parameterization used (Horinouchi et al. 2003) and to vertical resolution in the stratosphere (Boville and Randel 1992). It is nevertheless difficult to evaluate if these models reproduce SEWs realistically, because the SEWs are modulated by the QBO (Lott et al. 2009, Yang et al. 2012) and the QBO was absent from most of the models used in Horinouchi et al. (2003). Also, no studies have analysed the SEWs in coupled models, where the interplay between convection and ocean surface temperature is taken into account more consistently than in GCMs forced with prescribed sea surface temperatures.

Because the significance of the stratosphere for the global climate is now well established, several Earth system models (ESMs) participating in CMIP5 attempt to improve their representation of the stratosphere by extending their model higher and including the relevant additional physics. Among these models, four simulate a QBO: the Max-Planck Institute's model MPI-MR (Giorgetta et al. 2006), the CMCC model CMCC-CMS (Manzini et al. 2012), the Met Office's model HadGEM2-CC (Hardiman et al 2010), and the JAMSTEC model MIROC-ESM (Watanabe et al. 2011). These models with a well represented stratosphere and a QBO have a large number of vertical levels (see Table 1), and also non-orographic gravity wave drag parameterization schemes. It is generally recognized that in these models the parameterized gravity waves contribute at least as much as the resolved waves to the QBO forcing (Giorgetta et al. 2006). In this sense they are consistent with early theories of the QBO (Lindzen and Holton 1968) and with more recent observations (Ern and Preusse 2009). Some models for CMIP5 also have a reasonable stratosphere but vertical resolutions that are insufficient to simulate a QBO. In this paper, we will consider five of these models: the Meteorological Research Institute model MRI-CGCM3 (Yukimoto et al. 2011), the Max-Planck Institute's model MPI-LR, the two IPSL models IPSL-CM5B and IPSL-CM5A (Hourdin et al. 2013, Dufresne et al. 2013), and the Canadian Center for Climate Modeling and Analysis model CanESM2 (Arora et al. 2011, von Salzen et al. 2013). The total number of models considered is quite limited but it was considered desirable for the analysis to compare roughly the same number of models with and without a QBO. Another more practical constraint on the number of models used is the large amount of daily data required for the composite analysis.

Most of the studies that compare the SEWs between different stratospheric models are essentially based on spectral analysis (Horinouchi et al. 2003, Fujiwara et al. 2012) and provide little description of the spatio-temporal evolution of these waves. In this sense they are less comprehensive than the corresponding studies of CCEWs in the troposphere where characteristic patterns are often extracted via composite or regression techniques (e.g. Straub et al. 2010). Such techniques have been applied to SEWs in re-analysis data by Lott el al. (2009) or Yang et al. (2012), and allow to extract signals that compare very well in shape and amplitude with the unfiltered signals that modulate the day-to-day variability of the horizontal wind and temperature fields (compare for instance the temperature signal between unfiltered data during a given period and the composite in the Figs. 3b and 4b of Lott et al. 2009). For this comparison to make sense, the re-construction has to take into account that the SEWs travel in packets with a finite time life-cycle. All these aspects need to be sufficiently realistic to properly represent the breaking of the waves or their impact on dehydration. Also, spectral analysis can be misleading when focused on one process. For instance, if we are interested in the action of the wave on the zonal mean-flow by focusing on a spectral analysis of the EP-fluxes (as done in Horinouchi et al. 2003), it may be concluded that a given model underestimates some waves. However, as shown in Maury et al. (2013) the same model can still have a realistic wave signature on other fields such as temperature, which is essential if we are interested in dehydration. More fundamentally, it is also important to verify that a spectral signature attributed to Kelvin waves in a given field, also has a pattern that corresponds to Kelvin wave packets when extracted and reconstructed.

The purpose of this paper is to conduct such spectral and composite analyses on a subset of models participating in CMIP5. First, a spectral analysis of tropospheric and stratospheric fields is made to evaluate the models' ability to reproduce CCEWs and SEWs. Second, a composite analysis of the waves is performed using the method introduced in Lott et al. (2009). All results are presented according to the models ability to simulate the QBO and the precipitation variability.

2. Datasets and methodology

2.1. Datasets

All the data used in this paper are from the 9 ESMs which participated in CMIP5 and that were listed in the introduction (see also Table 1). These 9 models have a lid near or above the stratopause (around 1hPa) and therefore include a stratosphere (see Charlton-Perez et al. 2013 for details), but they vary considerably in their horizontal and vertical resolution. Of these 9 models, the 4 that simulate a QBO are also those with the largest number of levels in the vertical. In all the following figures these 4 models appear in the left column and the 5 models that do not simulate a QBO appear in the right column (following the order already given in Table 1). Note also that one model, the MRI-CGCM3 model, has a finer horizontal resolution than the other models. Note also that the CanESM2 model has a lid very close to the stratopause, significantly lower than in the other models, and this may affect the waves in the low stratosphere via reflections or damping near the model top. There are two models from the Max-Planck Institute which differ in terms of vertical resolution in the stratosphere and in the treatment of the ocean (Giorgetta et al. 2012). The high-resolution model (MPI-MR) simulates a QBO whereas the low resolution model (MPI-LR) does not (Giorgetta et al. 2002). The increased vertical resolution in MPI-MR could also help the model to more accurately simulate the vertical propagation of the waves. There are also two models from IPSL (IPSL5A and IPSL5B) that differ in their treatment of atmospheric turbulence, convection and clouds (Dufresne et al. 2013). As a consequence, the IPSL5B model has a much stronger and more realistic precipitation variability in the tropics than IPSL5A. An advantage of the present study over previous studies on convective parameterization and stratospheric waves, is that the two IPSL models differ only in few parameterizations (as in Scinocca et al. 2004), and the differences are such that the two models have realistic mean precipitation climatologies (they were both tuned for participation in CMIP5).

For each model we take the daily fields from the simulations covering the 50 years 1950-2000. The precipitation and the wind (u, v) on the 850hPa level are used to characterize

the variability in the lower troposphere and the temperature and winds on the 50hPa level to characterize the waves in the lower stratosphere. For validation, we will use the daily data from the GPCP datasets (Adler et al. 2003) for precipitation and from the ERAI reanalysis (Dee et al. 2011) for all the other fields. For ERAI we will consider 30 years ($1980-2010$) and for GPCP 13 years ($1997-2010$).

2.2. Methodology

To analyse the equatorial waves and their relation to convection we begin by following Wheeler and Kiladis (1999) and Hendon and Wheeler (2008) among others, and make space-time spectra of tropical signals. For precipitation, the spectra are displayed using an energy conserving formalism with log-axis and are superimposed on the spectral squared coherencies between the dynamical fields and the precipitation fields: these two techniques allow us to highlight the tropospheric CCEWs without needing to normalize the spectra with red-noise backgrounds (see Hendon and Wheeler 2008). On top of this, and following Lott et al. (2009) or Maury et al. (2013), we will analyze spectra of fields which are first tapered by a cosine function centered at the equator and crossing the zero line at $\pm 10^o$ and then averaged over the latitudinal band (10^oS-10^oN). We will also compute spectra of anti-symmetric precipitations by simply replacing the cosine taper with a sine taper of the same width before averaging in latitude.

Example spectra from ERAI at 50hPa are shown in Fig. 1 (further details on the method are given in the figure caption). The left panel shows the westward part of meridional wind (v) symmetric spectrum and the right panel shows the eastward part of zonal wind (u) symmetric spectrum. The relative broadband maxima in these two panels are the signatures of the Rossby gravity waves and of the Kelvin waves respectively (Lott et al. 2009).

To characterize the spatial structure and the life cycle of the SEWs we follow Lott et al. (2009) and make a composite analysis of band-pass filtered fields. For the Kelvin waves, the band pass filter operates in the frequency-wavenumber Fourier space, by multiplying the Fourier components of all fields by the transfer function shown in the right panel of Fig. 1. In this Figure, we see that the filter largely contains the broadband spectral maxima associated with Kelvin waves in ERAI, which guarantees that the filtered fields include them well. To finalize the filtering we then return to physical space. To diagnose when a Kelvin wave is present at 50hPa, we evaluate an index whose value equals the maximum of the filtered zonal wind averaged in latitude between 10^oS and 10^oN, and identify the longitude λ_M at which this maximum occurs. The composites are centered on the λ_Ms and built from averages over dates when maxima of this index exceed a given threshold. In each dataset the threshold is chosen so that around one event every two years is selected. We choose here to select a rather low number of events to guarantee independence between the selected wave packets, bearing in mind that each wave packet can have a life cycle that lasts near a month. Since this number is rather small, we have verified that none of our results are affected by moderate changes in the thresholds, provided that about the same number of dates are selected in each model (not shown). For the Rossby-gravity waves, we follow the same procedure but use the transfer function in the left panel of Fig. 1 to build the band pass filter, and use the meridional wind v to define the index.

Figure 2 shows the indices for Kelvin waves and Rossby-gravity waves, together with the temporal evolution of the zonal mean zonal wind at 50hPa. The Kelvin wave signal in zonal wind can exceed 10m/s in some models (black lines), and the Rossby-gravity signal in the meridional wind can exceed 5m/s (grey line). Some models show signals that are larger than in the reanalysis (Fig. 2a), but it is important to recall that in the re-analysis fields the equatorial waves can be underestimated (Ern et al. 2008) and can vary a lot from one re-analysis to the other (at 100hPa, see Fujiwara et al. 2012). Another interesting fact is that these signals vary from one model to the other and are substantially modulated by the QBO (see the left panels). There is a tendency, in models that simulate a QBO and in ERAI, to produce a larger Kelvin wave index when the QBO at 50hPa is westward, and a larger Rossby-gravity wave index when the QBO is eastward. As a consequence the composite method in the models with a QBO tends to pick dates when the QBO is westward/eastward at 50hPa for Kelvin/Rossby-gravity waves (see Lott et al. 2009 and the composite values for the zonal mean zonal wind at 50hPa in Table 1).

3. Kelvin waves

3.1. Spectral analysis

3.1.1. Precipitation and tropospheric winds

Spectra from the symmetric precipitations are presented in Fig. 3. The first five models capture quite well the magnitude of the variability of both the westward and eastward directions (Figs. 3b, 3c,3d, 3e, and 3f). The remaining four models in this figure (Figs. 3g, 3h, 3i, and 3j) underestimate this magnitude. Among the five models with quite realistic variability, four (3b, 3c,3d, 3i) also have relative maxima in the precipitation spectra that are near the dispersion curves of the equatorial Kelvin waves (thick solid lines on the right panels in all the subfigures). In these 4 models, these relative maxima are also near where the coherency between the zonal wind at 850hPa and the precipitation are quite large: they represent quite well both the convectively coupled Kelvin waves and the overall precipitation variability. Among these 4 models, 3 show very similar structure of the precipitation variability (Figs. 3c, 3d, and 3e), which naturally follows that they share an ECHAM based atmospheric component. This is quite interesting in that it offers an opportunity to isolate differences that come from the treatment of the stratosphere alone. One of the models with large precipitation variability has almost no contribution from the CCEWs to its variability (Figs. 3f).

Among the 4 models with insufficient variability (3g, 3h, 3i, 3j), two have some signature of CCEWs (Figs. 3g, 3i) and two have little or no CCEWs (Figs. 3h and 3j). Finally, it is useful to note that the IPSL model CM5B-LR has large precipitation variability and small convectively coupled Kelvin waves in Fig. 3f whereas the IPSL model CM5A-LR in Fig. 3h has weak precipitation variability and weak convectively coupled waves. This is also interesting in that it offers an opportunity to isolate differences that come from the precipitation variability alone.

To summarize, we find a lot of contrast between different models' ability to simulate convectively coupled Kelvin waves, which is consistent with the CMIP3 analysis of Straub et al. (2010). We also find a lot of difference in their ability to represent the overall variance of precipitation. Note again that in Fig. 3 the models are classified in order of decreasing precipitation variability from top to bottom, after placing the models with a QBO on the left, and those without on the right. This is also the order that was already adopted in Table 1 and that we will keep all along the paper.

3.1.2. Stratospheric wind

To identify the spectral domain in which Kelvin waves modulate the lower stratosphere the spectra for the zonal wind at 50hPa are shown in Fig. 4. In it we see that all the spectra have substantial power with well defined maxima in both the eastward and westward directions. In the westward direction, we know from Lott et al.(2009) that a good part of

the signal is due to the free planetary waves and is therefore related to the extra-tropics. We will not discuss this further. In the eastward direction all models have substantial signatures of Kelvin waves, with larger amplitude for models with a QBO. For presentation purposes, the contour interval has been made 4 times larger in the eastward panels for models with a QBO (Figs. 4c, 4e, 4g, and 4i). The essential role of QBO filtering is illustrated by noting that, of the models with a QBO, the smallest stratospheric Kelvin wave signal (Fig. 4g) still has more Kelvin wave power than the model with the largest Kelvin wave signal in the group of models without a QBO (Fig. 4d). When we look also from top to bottom, we see that the models with larger precipitation variability tend to have larger amplitude Kelvin waves in the stratosphere. Nevertheless, the differences between models are far less pronounced than their differences in terms of precipitation variability, which somehow mitigates the results in Horinouchi et al. (2003).

With respect to the influence of the precipitation variability, two factors suggest that the large-scale organization of convection by the CCEWs matters. First, the two models in Figs. 4f and 4h have almost identical stratospheric Kelvin waves, whereas their differences in precipitation variability are very large (Figs. 3f and 3h). As they both under-represent the CCEWs this suggests that differences in precipitation variability only matters if they occur in a spectral domain that is not too far from that of the stratospheric Kelvin waves. For this to occur, having CCEWs certainly helps. Second, the models with QBO in Figs. 4g-4i have quite substantial stratospheric Kelvin waves and quite small precipitation variability. This variability is nevertheless quite well placed between the dispersion curves corresponding to the CCEWs (Figs. 3g-3i).

3.2. Composite analysis

To characterize the spatial structure of Kelvin-wave life cycles, Fig. 5 presents longitude-time composites of the zonal wind at the equator. It is seen that all models simulate substantial eastward propagating disturbances with wind maxima often reaching 5m/s and more. Models with a QBO have a stronger Kelvin wave signal, and this signal moves faster eastward than in the reanalysis and in the models without a QBO. If we return to the zonal mean zonal winds and the 50hPa Kelvin wave indexes in Fig. 2, or to the zonal mean zonal wind composite values in Table 1, these excessively fast waves in the models with a QBO seem to be a consequence of the fact that these models tend to have an eastward bias. That is, during the dates selected to build the composite, the zonal wind is larger (more eastward) than in the models with no QBO and in ERAI (see Table 1). In contrast, in the models without a QBO, the wave signal moves at about the same phase speed as in ERAI. This is because in these models the zonal mean zonal wind at the equator is always westward, and with values near the observed values of the zonal mean zonal wind in the westward QBO phase (remember that in ERAI the dates selected to build the composite are essentially during westward QBO phase, Table 1).

These differences of phase speed in the stratosphere are consistent with the linear Kelvin wave theory in that waves with higher intrinsic phase speeds have larger vertical wavelengths and can propagate better vertically. In models with a QBO, the 50hPa winds during the selected events are more eastward than in ERAI or in models without a QBO (see the 4th column in Table 1). Therefore the 50hPa Kelvin waves in the models with a QBO need to have larger horizontal phase speeds to result in the same vertical propagation conditions as ERAI. In other words, the Kelvin waves with low phase speed have dissipated more in the models with a QBO because their intrinsic phase speed is lower than in the models without a QBO.

The winds and temperature composites at 0-day lag in Fig. 6 confirm that we are well in the presence of Kelvin waves, with the disturbance horizontal wind being zonal and in quadrature with the temperature. Again, we see that the signal in temperature is quite substantial, reaching more than 3K. An interesting fact is that in amplitude the temperature signals are quite identical when we compare models with a QBO and models without. This is somehow in contradiction with the differences in zonal winds between models in Fig. 5, and cannot simply be explained by a Doppler effect. In fact, from linear wave theory since the zonal wind and temperature fields due to Kelvin waves are both proportional to the geopotential divided by the intrinsic phase speed, the amplitude of the temperature signal should vary as that of the zonal wind.

Finally, it is also worth mentioning here that the two models in Figs. 5b) and 5j) stand out from the others in the sense that they have quite small Kelvin waves signals. The first is characterized by its very fine horizontal resolution, and the second by its rather low top.

4. Rossby gravity waves

4.1. Spectral analysis

4.1.1. Precipitation and tropospheric winds

The spectra of anti-symmetric precipitation also differ between models (Fig. 7). As for the symmetric precipitations in Fig. 3, the first five 5 models presented in this figure (7b, 7c, 7d, 7e, and 7f) have substantially larger variabilities than the four others. These five models also have larger variability than is observed (Fig. 7a), and this was not the case for the symmetric spectra. This difference between the symmetric and anti-symmetric results indicates that the simulated precipitation field is "whiter" than observed, and that the first five models have a tendency to produce a less organized precipitation variability at the large scale. This lack of large-scale organization is further indicated by the fact that the GPCP spectrum in Fig. 7a has a well defined relative maximum between the dispersion curves of the Rossby-gravity waves, and where the coherency with the meridional wind at 850hPa is also quite high. This indicates that convectively coupled Rossby-gravity waves organize a substantial part of the precipitation variability. This behavior is not well simulated by the models. On the one hand, a good part of them have enhanced coherency between precipitation and winds as indicated by the shaded zones between the dispersion curves for Rossby-gravity waves in Figs. 7b, c, d, and 7e. On the other hand these enhanced coherencies do not correspond to relative maxima in the precipitation spectra. This indicates that, while there is some interactions between precipitation and dynamics in the Rossby gravity wave spectral domain of the models, these interactions do not contribute to the precipitation variability as much as suggested by the observations.

As for the symmetric precipitation, we also find that for the model with large precipitation variability in Fig. 7f the large scale waves do not contribute much to the variability. In the two models with quite low precipitation variability (Figs. 7g and 7i) signatures of CCEWs are present, as indicated by the enhanced coherencies in the spectral domain of the Rossby-gravity waves.

4.1.2. Stratospheric winds

At 50hPa, models with a QBO have much more meridional wind variability than those without a QBO (Fig. 8, where for presentation purpose the contour interval used for the 3 models with a QBO in 8c, 8e, and 8i has been made four times larger than the contour interval used in the other models). In all the models with a QBO (Fig. 8c, e, g, h), the relative maxima are quite well located near the dispersion

curves of the Rossby gravity waves, and in agreement with ERAI in Fig. 8a. In the models without a QBO, the relative maxima are either too small in amplitude (Figs. 8b, f, h) or clearly in error in terms of location and shape (Figs. 8d, j). Again, from top to bottom, the differences between the meridional wind spectra in part follows from differences in convection variability. Here we say "in part" because this result is only clear when we compare the models with a QBO in the Figs. 8c,e to the models without a QBO in Figs. 8g,h. For the models without a QBO, the differences in the stratospheric spectra seem to be unrelated to differences in convection variability.

4.2. Composite analysis

The maps in Fig. 9 present longitude time-section of the composites of meridional wind at the equator. They show that all the models simulate westward propagating disturbances that shift continuously toward the east as expected for westward Rossby-gravity waves having eastward group velocity. As expected from the spectra, the waves have much larger amplitude and are more realistic in the models with a QBO than without. Again a sensitivity to convection is only apparent in the models with a QBO, with larger amplitude waves in the two models in Figs. 9c, 9e than in the two models in Figs. 9g, 9i. What seems more remarkable in Fig. 9 are the large differences in propagation characteristics. In most of the models the disturbances tend to have a much larger and negative phase speed than is seen in the observations, where it is near -13m/s (compare the phase lines slope to the dashed line). There is one exception, Fig. 9g where the disturbance propagates at about the observed phase speed indicated in Fig. 9a. Consistent with these differences, the groups of waves in the models propagate more slowly eastward than in ERAI, except again for the model in Fig. 9g where they propagate slightly faster (in all subfigures compare the amplitude displacement of the group of waves to the dotted lines). Note that this relatively fast group propagation in the model of Fig. 9g can not be explained in terms of stronger advection by the background wind since the composite zonal mean zonal wind of about +8m/s (see table 1) in this model is not much different from the composite zonal mean zonal wind found in the other models with a QBO. This slow eastward propagation bias in all but one QBO model becomes very pronounced when one looks to the models without a QBO. In these models the meridional wind oscillations almost stay confined within the same longitude bands as time evolves (Figs. 9b-9d-9f-9h-9i).

The composite maps for horizontal wind and temperature in Fig. 10 confirm that we are in presence of Rossby-gravity waves. The amplitude reach more than 1K in temperature for most models with a QBO (Figs. 10c, e, i), except again for the model in Fig. 10g where it is much smaller. It is also interesting that the signal in the models with a QBO is substantially larger than the signal in the reanalysis (except again for the model in Fig. 10g). Finally, it seems that the two models with a QBO and stronger convection variability (Figs. 10c, 10e) have larger wave amplitudes than the two with weaker convection variability (Figs. 10g, 10i). Nevertheless, this interpretation should be taken with care, since the model in Fig. 10g behaves here quite differently from the others, and since the model in Fig 10i has a quite reasonable Rossby-gravity waves signal. For the models without a QBO there are still coherent Rossby-gravity waves structures and this occurs despite the fact that the zonal mean zonal wind is negative in all of them (see table 1). This inherently yields a small amplitude intrinsic phase speed and hence more efficient vertical dissipation. Still in the models without a QBO the effect of convection variability is hard to detect, and this is particularly evident when we compare the two IPSL models in Figs. 10f and 10h again.

5. Conclusion

According to the subset of CMIP5 simulations considered in this paper, the simulation of the precipitation variability is still a major issue. More precisely, the spectral distribution of the precipitation variability and the contribution of the CCEWs to this variability differ significantly between models (Figs. 3 and 7). In this sense, the situation is not much better than for the models participating in CMIP3 and analyzed for instance in Straub et al. (2010). As we are here mostly interested in the stratosphere, this should impact the stratospheric waves according to Horinouchi et al. (2003), and partly because the convectively coupled Kelvin waves can emit substantial Kelvin waves in the stratosphere (Maury et al. 2013).

Despite these differences, most of the 9 models have substantial and quite realistic Kelvin waves and some Rossby gravity waves in the lower stratosphere. This shows that the relation between the stratospheric waves and the convection is more subtle than expected, suggesting that convection is not the only source of waves and that the dynamical filterings by the zonal wind and by the vertical resolution largely mitigate the differences between the models in terms of precipitation.

In general the models have little difficulties in simulating stratospheric Kelvin wave packets because these waves have a quite large vertical wavelength and a positive phase speed. In models without a QBO their propagation is favored by the fact that the zonal mean zonal wind is very often negative, which results in large intrinsic phase speed and large vertical wavelength. In models with a QBO this situation is only met roughly half of the time. Nevertheless, and despite the fact that the favorable conditions for the Kelvin wave propagation are less frequent in models with a QBO, we find that the models with a QBO have larger amplitude Kelvin waves than the models without (Fig. 4). The explanation of this apparent contradiction could be that the refined vertical resolution in the lower stratosphere needed to produce a QBO also helps to better resolve the Kelvin waves. A good illustration is the comparison between the two MPI models that only differ by their resolution in the stratosphere: the one with a QBO and refined vertical resolution has a stronger Kelvin wave signal than the other (Figs. 5c and 5d). This sensitivity of the Kelvin waves to the vertical resolution is probably one of the causes that models need such refined resolutions to produce a QBO. While it has been found that models without a QBO underestimate the stratospheric Kelvin waves, it must also be noted that some models without a QBO have about the right Kelvin wave signal in temperature and only underestimate the signal in zonal wind.

For Rossby-gravity waves, the differences between the models are much more pronounced than for Kelvin waves. For instance models without a QBO tend to produce very fast westward propagating Rossby gravity waves. In fact in these models, the Rossby gravity waves must have negative phase speeds that are inferior to the negative zonal mean zonal wind (see for instance the spectra in Fig. 8d, or the composites in the right column of Fig. 9). Also, the positive intrinsic group speed of the waves opposed the advection by the negative zonal mean zonal wind, and the Rossby-gravity wave packets tend to stay at the same place (right column of Fig. 9) instead of moving eastward (Fig. 9a). Of course many of the models without a QBO have problems in producing these waves coherently as illustrate the composites presented in Fig. 10 (right-hand column). For models with a QBO, the Rossby gravity waves are much better represented (see Figs. 9- 10) but there are big qualitative and

quantitative differences between the models. In three models with a QBO, the Rossby gravity waves have excessively strong westward phase speed but excessively weak eastward group speeds, while maintaining quite large amplitudes.

It emerges from this discussion that models differ significantly in their ability to represent large scale Kelvin and Rossby gravity wave packets in the lower stratosphere. Nevertheless, these differences are less related to the variability of convection than we would have expected from earlier papers (Horinouchi et al. 2003). This conclusion should nevertheless be moderated by the fact that we have only analysed here large scale waves. They are, however, consistent with more recent observational papers which show that the climatology of the wave activity in the tropical tropopause layer is not closely related to the tropospheric convection (Alexander and Ortland 2010). The differences between the models seem to be controlled more by the vertical resolution (Boville and Randel 1992). This probably follows that (i) the models with refined vertical scales likely induce less numerical dissipation of the vertically propagating waves (this is quite evident for the Kelvin waves), and that (ii) the models with high vertical resolution also have a QBO and simulate better the backgound wind conditions favorable to these waves (this is quite clear for the Rossby gravity waves). The fact that vertical resolution is really a crucial issue is further illustrated by the two models presented in the panels (b) and (j) in all our figures. These two models have problems in representing the large-scale equatorial waves, one is characterized by a quite high horizontal resolution, the other by a top that is quite low (at the stratopause).

Finally, our result that the influence of convection is not as large as we could have expected from past studies should be tempered by the fact that we did not look at the vertical distribution of the latent heating associated with precipitation and we know since Holton (1975) that this factor is essential to the efficiency of wave forcing. Also, the weak sensitivity to convection we found in the two IPSL models, which only differ by their treatment of the convection parameterization in the atmosphere, could well be due to that the two versions lack of convective variability near the spectral domain of the SEWs. It would therefore be very helpful to compare twin models that only differ in their representation of the CCEWs. In fact, even if CCEWs in part dissipate before reaching the stratosphere, their presence is certainly beneficial to inject coherent structure on the variabilities of precipitations at the large horizontal spatial scales and rather fast time scales of the Kelvin and Rossby gravity wave packets that propagate in the stratosphere.

Acknowledgement:

This work was supported by the European Commission's 7th Framework Programme, under the projects EMBRACE (Grant agreement 282672) and COMBINE (Grant agreement 226520), and by the ANR project STRADYVARIUS. GPCP Precipitation data are provided by the NOAA/OAR/ESRL PSD, Boulder, Colorado, USA, from their Web site at http://www.esrl.noaa.gov/psd/. S. Watanabe was supported by the SOUSEI program, MEXT, Japan, and his simulations were performed using the Earth Simulator.

References

Amodei, M., Pawson, S., Scaife, A. A., Langematz, U., Lahoz, W., Li, D. M., and Simon, P., 2001: The SAO and Kelvin waves in the EuroGRIPS GCMS and the UK Met. Office analyses, *Ann. Geophys.,* **19,** 99-114, doi:10.5194/angeo-19-99-2001.

Adler, R.F., G.J. Huffman, A. Chang, R. Ferraro, P. Xie, J. Janowiak, B. Rudolf, U. Schneider, S. Curtis, D. Bolvin, A. Gruber, J. Susskind, and P. Arkin, 2003: The Version 2 Global Precipitation Climatology Project (GPCP) Monthly Precipitation Analysis (1979-Present). *J. Hydrometeor.,* **4,**1147-1167.

Alexander, M.J. and D.A. Ortland, 2010: Equatorial waves in High Resolution Dynamics Limb Sounder (HIRDLS) data, *J. Geophys. Res.,* **115,** D24111, doi:10.1029/2010JD014782.

V.K. Arora, J. F. Scinocca, G. J. Boer, J. R. Christian, K. L. Denman, G. M. Flato, V. V. Kharin, W. G. Lee, and W. J. Merryfield, 2011: Carbon emission limits required to satisfy future representative concentration pathways of greenhouse gases, *Geophys. Res. Lett.,* **38,** L05805, doi:10.1029/2010GL046270.

Boville, B.A. and W.J. Randel, 1992: Equatorial waves in a stratospheric GCM: effects of the vertical resolution, *J. Atmos. Sci.,* **9,** 785–801.

Charlton-Perez, A. J., et al. ,2013: On the lack of stratospheric dynamical variability in low-top versions of the CMIP5 models, *J. Geophys. Res. Atmos.,* **118,** 2494-2505, doi:10.1002/jgrd.50125

Dee, D. P., Uppala, S. M., Simmons, A. J., Berrisford, P., Poli, P., Kobayashi, S., Andrae, U., Balmaseda, M. A., Balsamo, G., Bauer, P., Bechtold, P., Beljaars, A. C. M., van de Berg, L., Bidlot, J., Bormann, N., Delsol, C., Dragani, R., Fuentes, M., Geer, A. J., Haimberger, L., Healy, S. B., Hersbach, H., Holm, E. V., Isaksen, L., Kallberg, P., Kohler, M., Matricardi, M., McNally, A. P., Monge-Sanz, B. M., Morcrette, J.-J., Park, B.-K., Peubey, C., de Rosnay, P., Tavolato, C., Thepaut, J.-N. and Vitart, F., 2011: The ERA-Interim reanalysis: configuration and performance of the data assimilation system., *Q.J.R. Meteorol. Soc.*, **137:** 553–597. doi: 10.1002/qj.828.

Dufresne, J.-L., M.-A. Foujols, S. Denvil, A. Caubel, O. Marti, O. Aumont, Y. Balkanski, S. Bekki, H. Bellenger, R. Benshila, S. Bony, L. Bopp, P. Braconnot, P. Brockmann, P. Cadule, F. Cheruy, F. Codron, A. Cozic, D. Cugnet, N. de Noblet, J.-P. Duvel, C. Ethe, L. Fairhead, T. Fichefet, S. Flavoni, P. Friedlingstein, J.-Y. Grandpeix, L. Guez, E. Guilyardi, D. Hauglustaine, F. Hourdin, A. Idelkadi, J. Ghattas, S. Joussaume, M. Kageyama, G. Krinner, S. Labetoulle, A. Lahellec, M.-P. Lefebvre, F. Lefevre, C. Levy, Z. X. Li, J. Lloyd, F. Lott, G. Madec, M. Mancip, M. Marchand, S. Masson, Y. Meurdesoif, J. Mignot, I. Musat, S. Parouty, J. Polcher, C. Rio, M. Schulz, D. Swingedouw, S. Szopa, C. Talandier, P. Terray, N. Viovy and N. Vuichard, 2013: Climate change projections using the IPSL-CM5 Earth System Model: from CMIP3 to CMIP5, *Climate Dynamics,* **40,** no 9-10, 2123-2165, doi:10.1007/s00382-012-1636-1.

Ern, M., P. Preusse, M. Krebsbach, M. G. Mlynczak, and J. M. Russell, 2008: Equatorial wave analysis from SABER and ECMWF temperatures, *Atmos. Chem. and Phys.,* **8,** 845-869.

Ern, M., and P. Preusse, 2009: Quantification of the contribution of equatorial Kelvin waves to the QBO wind reversal in the stratosphere *Geophys. Res. Lett.*, **36,** L21801, DOI: 10.1029/2009GL040493.

Flannaghan, T.J., and S. Fueglistaler, 2013: The importance of the tropical tropopause layer for equatorial Kelvin wave propagation, *J. Geophys. Res.,* **11,**, 51605175. DOI: 10.1002/jgrd.50418

Fujiwara M., M. K. Yamamoto, H. Hashiguchi, T. Horinouchi, and S. Fukao, 2003: Turbulence at the tropopause due to breaking Kelvin waves observed by the Equatorial Atmosphere Radar, *Geophys. Res. Letters,* **30,** 4, 1171, doi:10.1029/2002GL016278.

Fujiwara, M., J. Suzuki, A. Gettelman, M. I. Hegglin, H. Akiyoshi, and K. Shibata, 2012: Wave activity in the tropical tropopause layer in seven reanalysis and four chemistry climate model data sets, *J. Geophys. Res.,* **117,** D12105, doi:10.1029/2011JD016808.

Garcia, R. R. and Salby, M. L., 1987: Transient response to localized episodic heating in the tropics. Part II: Far-field behavior., *J. Atmos. Sci.,***44,** 499–530, 1987.

Giorgetta, M. A., E. Manzini, and E. Roeckner, 2002: Forcing of the quasi-biennial oscillation from a broad spectrum of atmospheric waves, *Geophys. Res. Lett.,* **29(8),** doi:10.1029/2001GL014756.

Giorgetta, M. A., E. Manzini, E. Roeckner, M. Esch, and L. Bengston, 2006: Climatology and forcing of the quasi-biennial oscillation in the MECHAM5 model, *J. Climate,* **19,** 3882-3901.

Hendon, H. H., and M. C. Wheeler, 2008: Some space-time spectral analyses of tropical convection and planetary-scale waves, *J. Atmos. Sci.*, **65,** 2936-2948.

Hertzog, A., and F. Vial, 2001: A study of the dynamics of the equatorial lower stratosphere by use of ultra-long-duration balloons 2: Gravity waves, *J. Geophys. Res.,* **106,** 22,745–22,761.

Holton, J. R., 1972: Waves in the equatorial stratosphere generated by tropospheric heat sources, *J. Atmos. Sci.*, **29,** 368–375.

Horinouchi, T., S. Pawson, K. Shibata, E. Manzini, M.A. Giorgetta, F. Sassi, R. J. Wilson, K. Hamilton, J. DeGrandpe and A.A. Scaife, 2003: Tropical cumulus convection and upward propagating waves in middle-atmospheric GCMs, *J. Atmos. Sci.*, **60,** 2765–2782.

Lindzen, R. S., and J. R. Holton, 1968: A theory of the quasi-biennial oscillation, *J. Atmos. Sci.,* **25,** 1095–1107.

Lott, F., J. Kuttippurath, and F. Vial, 2009: A Climatology of the Gravest Waves in the Equatorial Lower and Middle Stratosphere: Method and comparison between the ERA-40 re-analysis and the LMDz-GCM, *Journal of the Atmospheric Sciences,* **66**, 1327–1346, 2009.

Manzini, E., and K. Hamilton, 1993: Middle Atmospheric Traveling Waves Forced by Latent and Convective Heating. *J. Atmos. Sci.*, **50**, 2180–2200.

Manzini, E., C. Cagnazzo, P. G. Fogli, A. Bellucci, and W. A. Muller, 2012: Stratosphere-troposphere coupling at inter-decadal time scales: Implications for the North Atlantic Ocean, *Geophys. Res. Lett.,* **39,** L05801, doi:10.1029/2011GL050771

Martin G. M., N. Bellouin, W. J. Collins, I. D. Culverwell, P. R. Halloran, S. C. Hardiman, T. J. Hinton, C. D. Jones, R. E. McDonald, A. J. McLaren, F. M. O'Connor, M. J. Roberts, J. M. Rodriguez, S. Woodward, M. J. Best, M. E. Brooks, A. R. Brown, N. Butchart, C. Dearden, S. H. Derbyshire, I. Dharssi, M. Doutriaux-Boucher, J. M. Edwards, P. D. Falloon, N. Gedney, L. J. Gray, H. T. Hewitt, M. Hobson, M. R. Huddleston, J. Hughes, S. Ineson, W. J. Ingram, P. M. James, T. C. Johns, C. E. Johnson, A. Jones, C. P. Jones, M. M. Joshi, A. B. Keen, S. Liddicoat, A. P. Lock, A. V. Maidens, J. C. Manners, S. F. Milton, J. G. L. Rae, J. K. Ridley, A. Sellar, C. A. Senior, I. J. Totterdell, A. Verhoef, P. L. Vidale, and A. Wiltshire, 2011: The HadGEM2 family of Met Office Unified Model Climate configurations, *Geosci. Model Dev. Discuss.,* **4,** 765–841, doi:10.5194/gmdd-4-765-2011.

Maury, P. and F. Lott, 2013: On the presence of equatorial waves in the lower stratosphere of a general circulation model, *Atmospheric Chemistry and Physics Discussion,* **13,** 22607–22637. doi:10.5194/acpd-13-22607-2013

Maury, P. , F. Lott, L. Guez, and J.-P. Duvel, 2013: Tropical variability and stratospheric equatorial waves in the IPSLCM5 model, *Climate Dynamics,***40,** 2331–2344. DOI 10.1007/s00382-011-1273-0.

Mote P. W., T. J. Dunkerton, and D. Wu, 2002: Kelvin waves in stratospheric temperature observed by the Microwave Limb Sounder, *J. Geophys. Res.,* **107,** doi:10.1029/2001JD001056.

Mote, P. W., and T. J. Dunkerton, 2004: Kelvin wave signatures in stratospheric trace constituents, *J. Geophys. Res.,* **109,** D03101, doi:10.1029/2002JD003370.

Randel W. J., and J. C. Gille, 1991: Kelvin Wave Variability in the Upper Stratosphere Observed in SBUV Ozone Data, *J. Atmos. Sci.*,**48**, 2330–2349.

Randel W. J., and F. Wu, 2005: Kelvin-wave variability near the equatorial tropopause observed in GPS radio occultation measurements, *J. Geophys. Res.,* **110,** D03102, doi: 10.1029/2004JD005006.

Rodgers, C. D., 1976: Evidence for the five-day wave in the upper stratosphere, *J. Atmos. Sci.*,**33**, 710–711.

Salby, M.L., D.L. Hartmann, P.L. Bailey, and J.C. Gille, 1984: Evidence for equatorial Kelvin modes in NIMBUS-7 LIMS, *J. Atmos. Sci.*,**41**, 220-235.

Scinocca, J.F. and N.A. McFarlane, 2004: The Variability of Modelled Tropical Precipitation,*J. Atmos. Sci.*, **61**, 1993–2015.

von Salzen, K., J. F. Scinocca, N. A. McFarlane, J. Li, J. N. S. Cole, D. Plummer, M. C. Reader, X. Ma, M. Lazare, L. Solheim, 2013: The Canadian Fourth Generation Atmospheric Global Climate Model (CanAM4). Part I: Physical processes, *Atmosphere-Ocean,***51,** doi:10.1080/07055900.2012.755610

Sassi M. N. and coauthors, 2003: A study of equatorial waves characteristics using rockets, balloons, Lidar and Radar, *Adv. Spa. Res.,* **5,** 813–818. doi:10.1016/S0273-1177(03)00412-5.

Straub, K.H., P.T. Haertel, and G.N. Kiladis, 2010: An analysis of convectively coupled Kelvin waves in 20 WCRP CMIP3 global coupled climate models, *Journal of Climate,***23,** 3031–3056.

Tsuda T., Y. Murayama, H. Wiryosumarto, S.W.B. Harijono, and S. Kato, 1994: Radiosonde observations of equatorial atmosphere dynamics over Indonesia, 1: Equatorial waves and diurnal tides, *J. Geophys. Res.,* **99,** 10591-10516.

Vial, F., A. Hertzog, C. R. Mechoso, C. Basdevant, P. Cocquerez, V. Dubourg, and F. Nouel, 2001: A study of the dynamics of the equatorial lower stratosphere by use of ultra-long-duration balloons 1: Planetary scales, *J. Geophys. Res.,* **106,** 22,725-22,743.

Wallace, J. M., and V. E. Kousky, 1968: Observational evidence of Kelvin waves in the tropical stratosphere, *J. Atmos. Sci.*, **25,** 900-907.

Watanabe, S., Hajima, T., Sudo, K., Nagashima, T., Takemura, T., Okajima, H., Nozawa, T., Kawase, H., Abe, M., Yokohata, T., Ise, T., Sato, H., Kato, E., Takata, K., Emori, S., and Kawamiya, M.: MIROC-ESM 2010: model description and basic results of CMIP5-20c3m experiments, *Geosci. Model Dev.,* **4,** 845-872, doi:10.5194/gmd-4-845-2011

Wheeler, M., and G. N. Kiladis, 1999: Convectively coupled equatorial waves: analysis of clouds and temperature in the wavenumber-frequency domain, *J. Atmos. Sci.*, **56,** 375-399.

Wheeler, M., G. N. Kiladis and P. J. Webster, 2000: Large-scale dynamical fields associated with convectively coupled equatorial waves, *J. Atmos. Sci.*, **57,** 613–640.

Yang, Gui-Ying, Brian Hoskins, Lesley Gray, 2012: The Influence of the QBO on the Propagation of Equatorial Waves into the Stratosphere, *J. Atmos. Sci.,* **69,** 2959–2982. doi: http://dx.doi.org/10.1175/JAS-D-11-0342.1

With QBO					Without QBO				
Name:	Resolution	Top	Kelvin	RG	Name:	Resolution	Top	Kelvin	RG
a) ERAI	T255L60	10Pa	-17m/s	9m/s	b) MRI-CGCM3	T159L48	1Pa	-5m/s	-5m/s
c) MPI-MR	T63L95	1Pa	-1m/s	14m/s	d) MPI-LR	T63L47	1Pa	-10m/s	-11m/s
e) CMCC	T63L95	1Pa	2m/s	9m/s	f) IPSLCM5B	96x78xL39	5Pa	-9m/s	-10m/s
g) HadGEM2-CC	192x144xL60	1Pa	-11m/s	8m/s	h) IPSLCM5A	96x78xL39	5Pa	-10m/s	-11m/s
i) MIROC-ESM	T42L80	.3Pa	-3m/s	5m/s	j) CanESM2	128x64xL35	1hPa	-3.5m/s	-4m/s

Table 1. List of models used with their resolutions and model tops. Also shown are the composite values of the zonal mean zonal wind corresponding to dates when Kelvin waves and Rossby gravity waves are extracted to build the composites

Yanai, M., and T. Maruyama, 1966: Stratospheric wave disturbances in the tropical stratosphere, *J. Meteor. Soc. Japan,* **44,** 291–294.

Yukimoto, S. , Y. Adachi, M. Hosaka, T. Sakami, H. Yoshimura, M. Hirabara, T. Y. Tanaka, E. Shindo, H. Tsujino, M. Deushi, R. Mizuta, S. Yabu, A. Obata, H. Nakano, T. Koshiro, T. Ose, and A. Kitoh, 2012: A New Global Climate Model of the Meteorological Research Institute: MRI-CGCM3-Model Description and Basic Performance, *Journal of the Meteorological Society of Japan,* **90A,** 23–64. DOI:10.2151/jmsj.2012-A02.

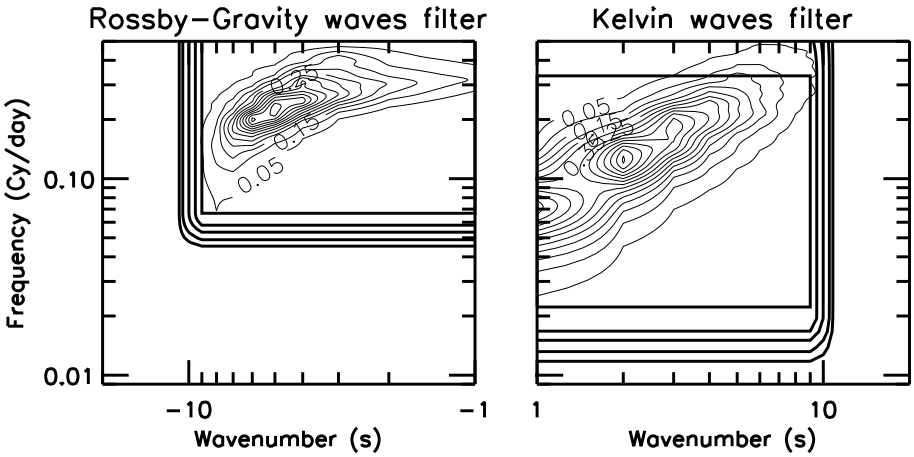

Figure 1. Left: Westward component of the 50hPa spectra of the meridional wind (thin solid) and transfer function used to extract the Rossby gravity waves (thick solid, contour interval=0.2). Right: Eastward component of the 50hPa spectra of the zonal wind and transfer function used to extract the Kelvin waves. For all models the filters are identical but the spectra shown here are from ERAI data. To estimate the spectra, the fields are tapered in latitude by a cos taper of 20^o width centered at the equator and then averaged in latitude over the equatorial band. Each year a time-longitude periodogram is then made and the spectra is estimated by averaging the periodograms over the years. The estimate of the spectra is further smoothed by applying 30 times a 1-2-1 filter in the temporal domain. This smoothes the signal over around 15 points, yielding a spectral resolution of around 4.10^{-2}cy/d.

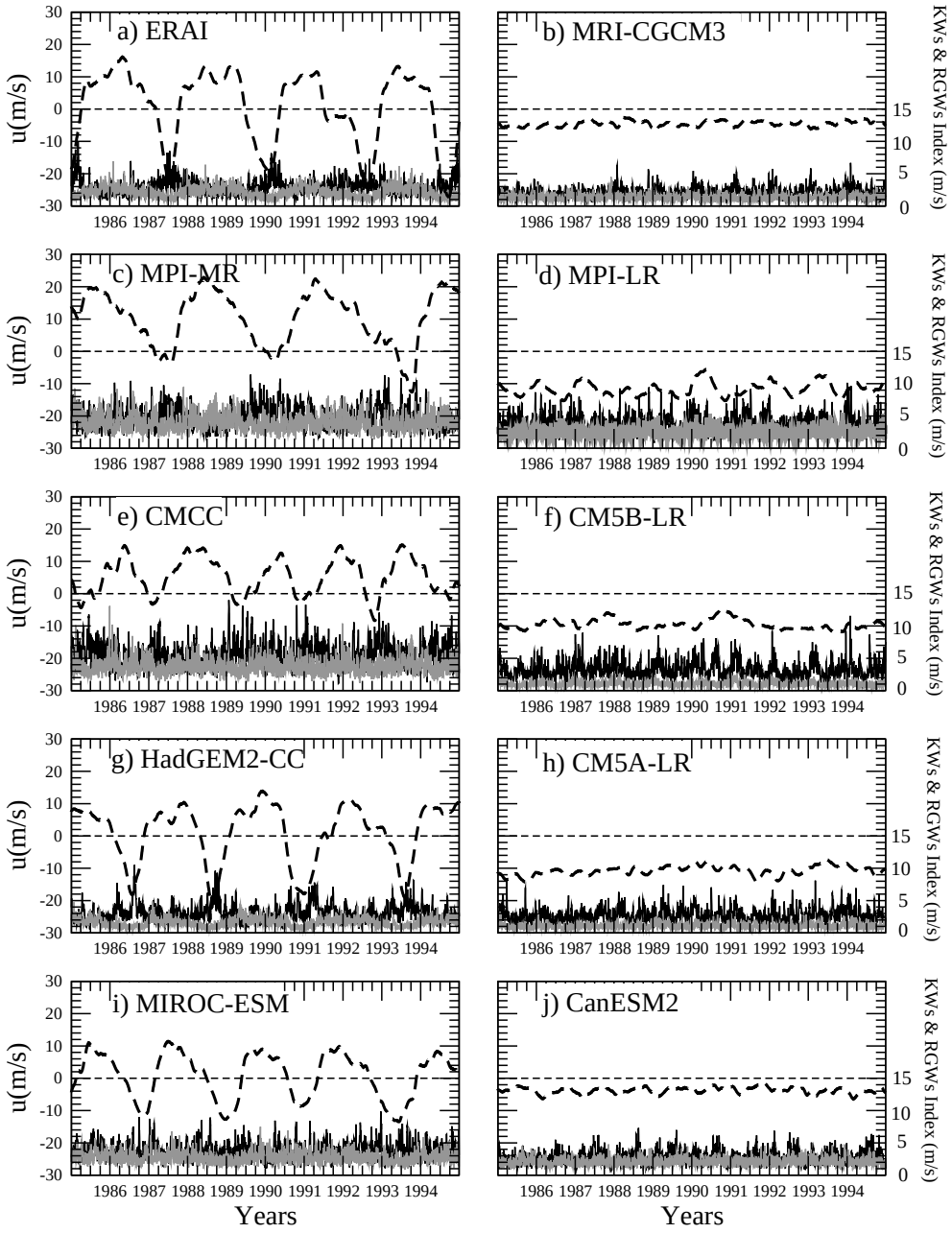

Figure 2. Zonal mean zonal wind at the Equator (dashed), Kelvin wave index (black), and Rossby-gravity waves index (grey). All series are built from 50hPa fields.

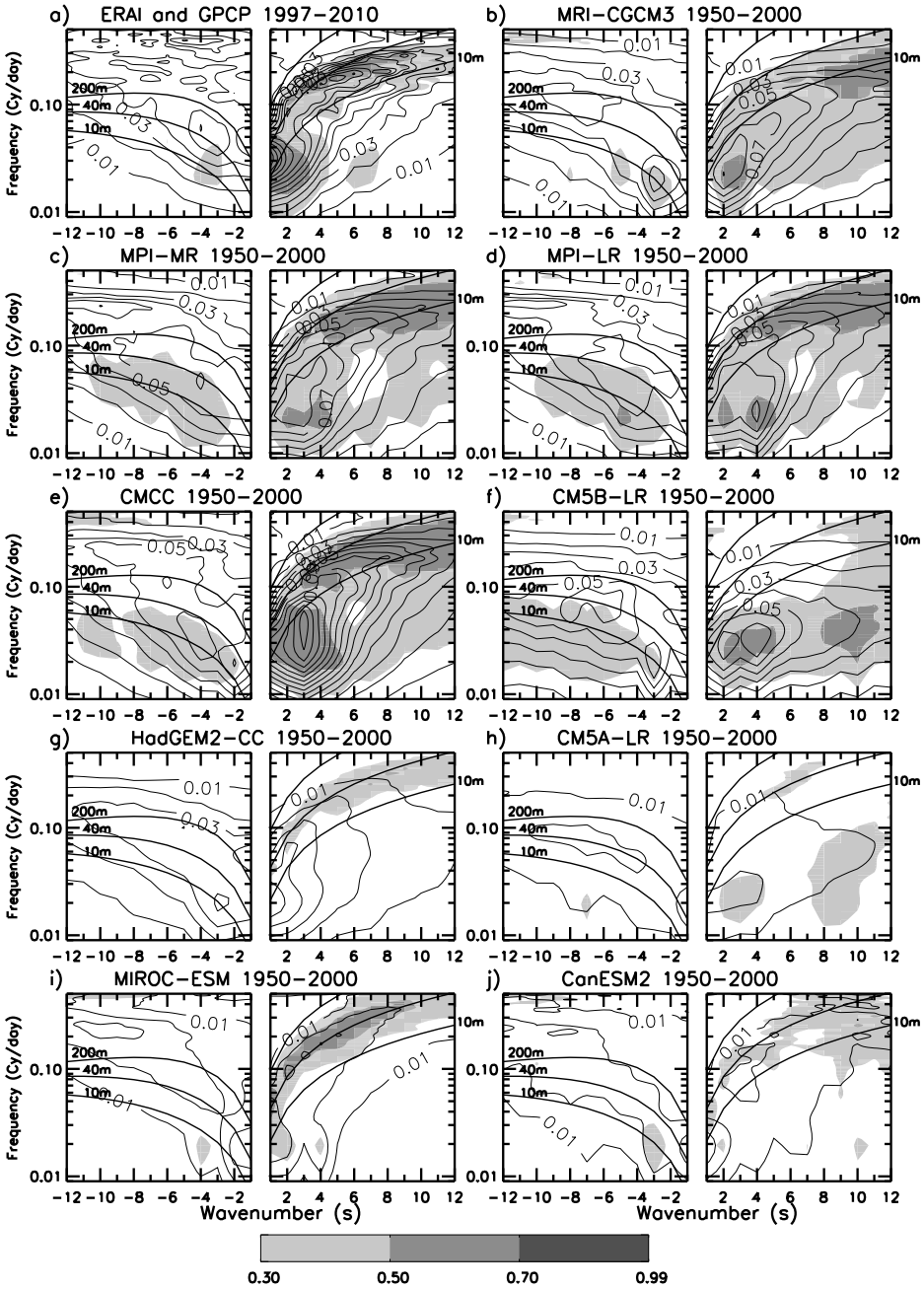

Figure 3. Spectra of symmetric precipitation (contour lines with interval=0.01mm^{2}day^{-3}) and of its squared coherency with the zonal wind at 850hPa (shaded). The precipitation and wind are first tapered by a cos function of 20^o width centered at the equator and averaged over (10^{o}S-10^{o}N) before their frequency-wavenumber periodograms are evaluated. The squared coherencies are then built from ratio between cross-spectra and spectra, those being estimated from averaged and smoothed yearly periodograms and cross periodograms exactly as described in Fig. 1. All the coherency levels shown are above the 99%-level (which is around 0.2 for $r = 50$ degrees of freedom). In all figures are also shown the dispersion curves for the $n = 1$ Rossby waves and Kelvin waves with equivalent depths $h = 10, 40, 200$m.

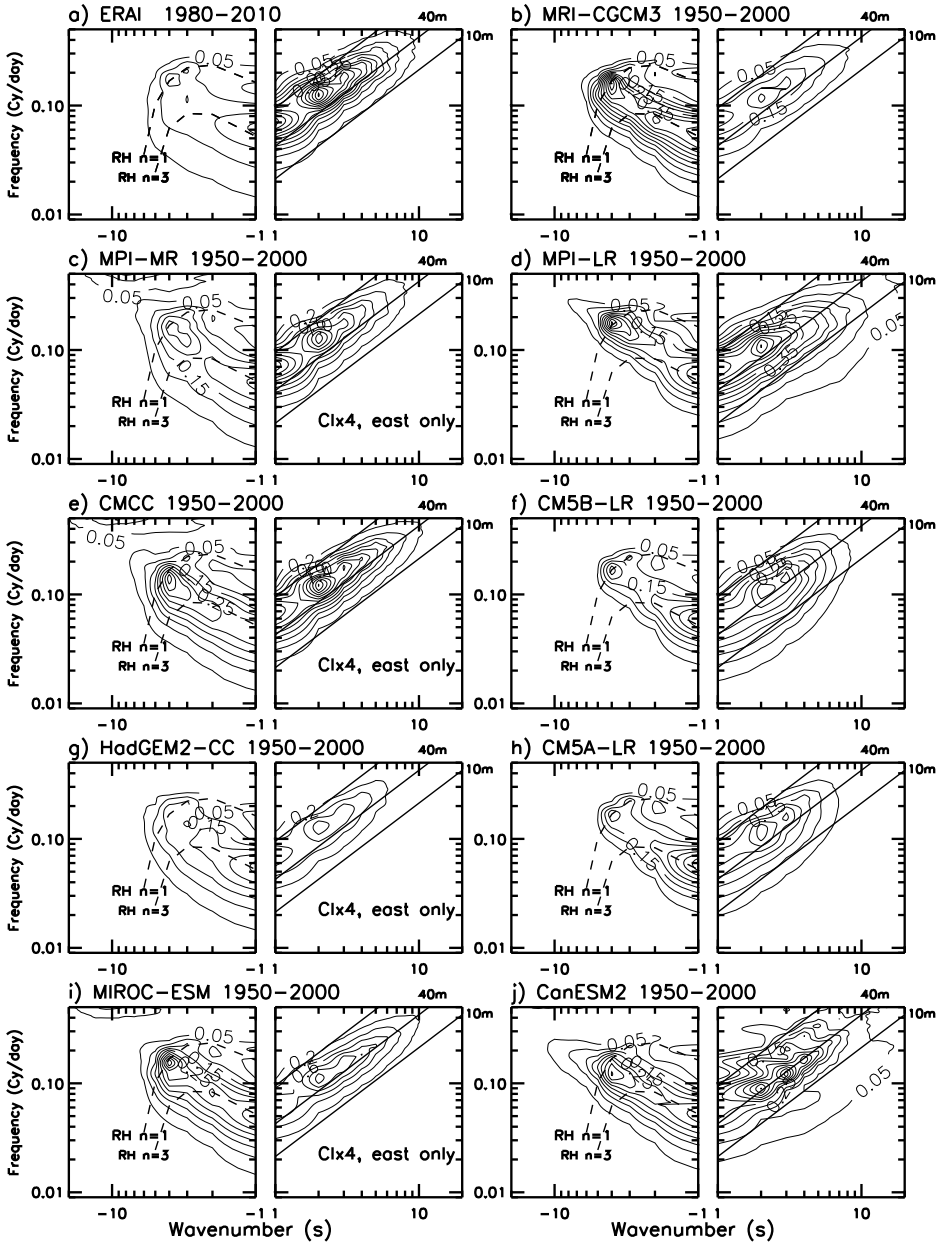

Figure 4. Spectra of the zonal wind at 50hPa tapered and averaged over the equatorial band as described in Fig. 1 (contour interval: $0.05\mathrm{m}^2\mathrm{s}^{-2}\mathrm{day}^{-1}$). The thick solid lines are for the Kelvin waves dispersion curves, whereas the dashed lines are for the free planetary waves dispersion curves with $n = 1, 3$ after application of a Doppler spread by an eastward wind $U = 15\mathrm{m/s}$ to take into account advection by the midlatitude winds.

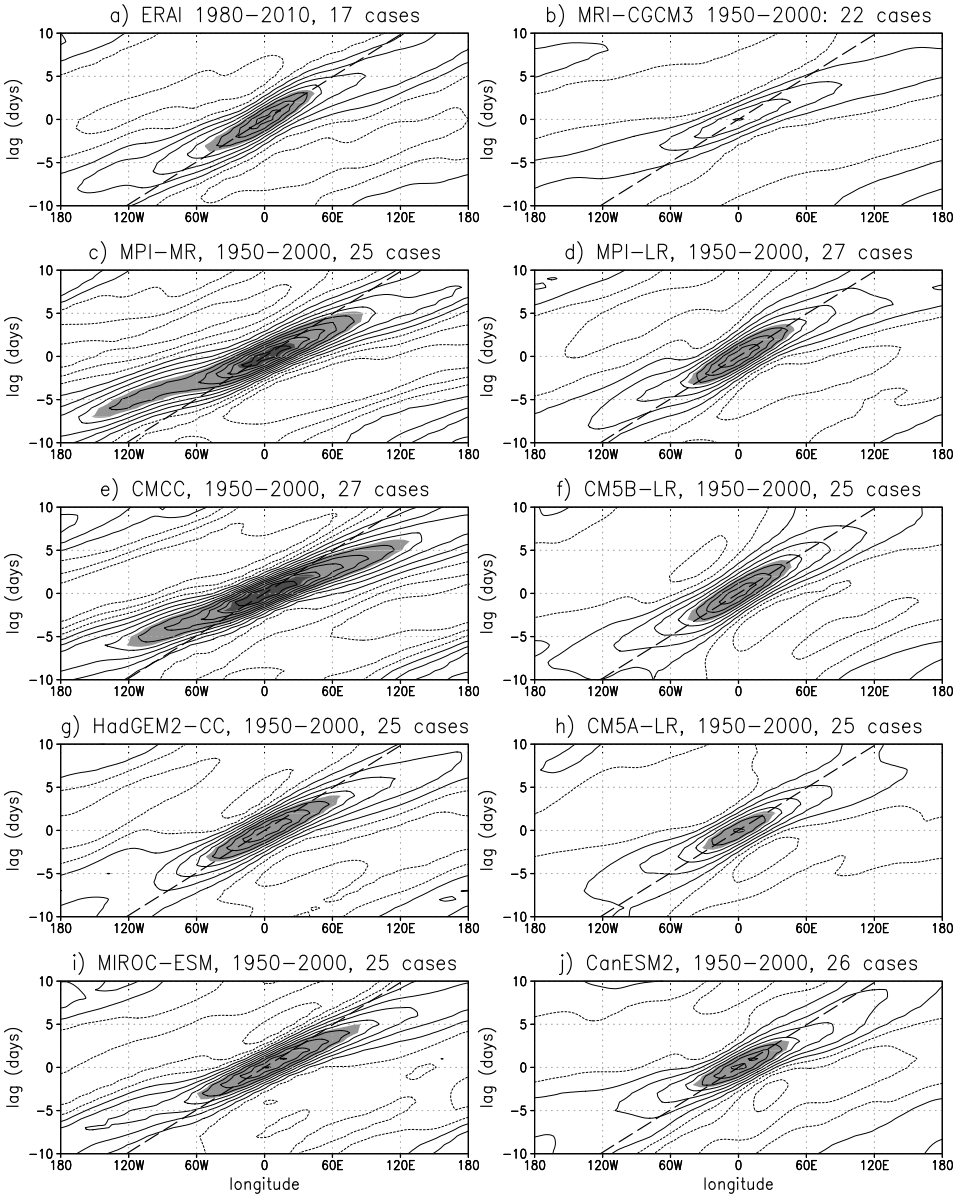

Figure 5. Time evolution of the zonal wind anomaly at the equator due to the passage of Kelvin waves at 50hPa, contour interval: 1.25m/s, values above 5m/s and 10m/s are in light grey and in dark grey respectively. The thick dashed line is for a uniform displacement at 15m/s.

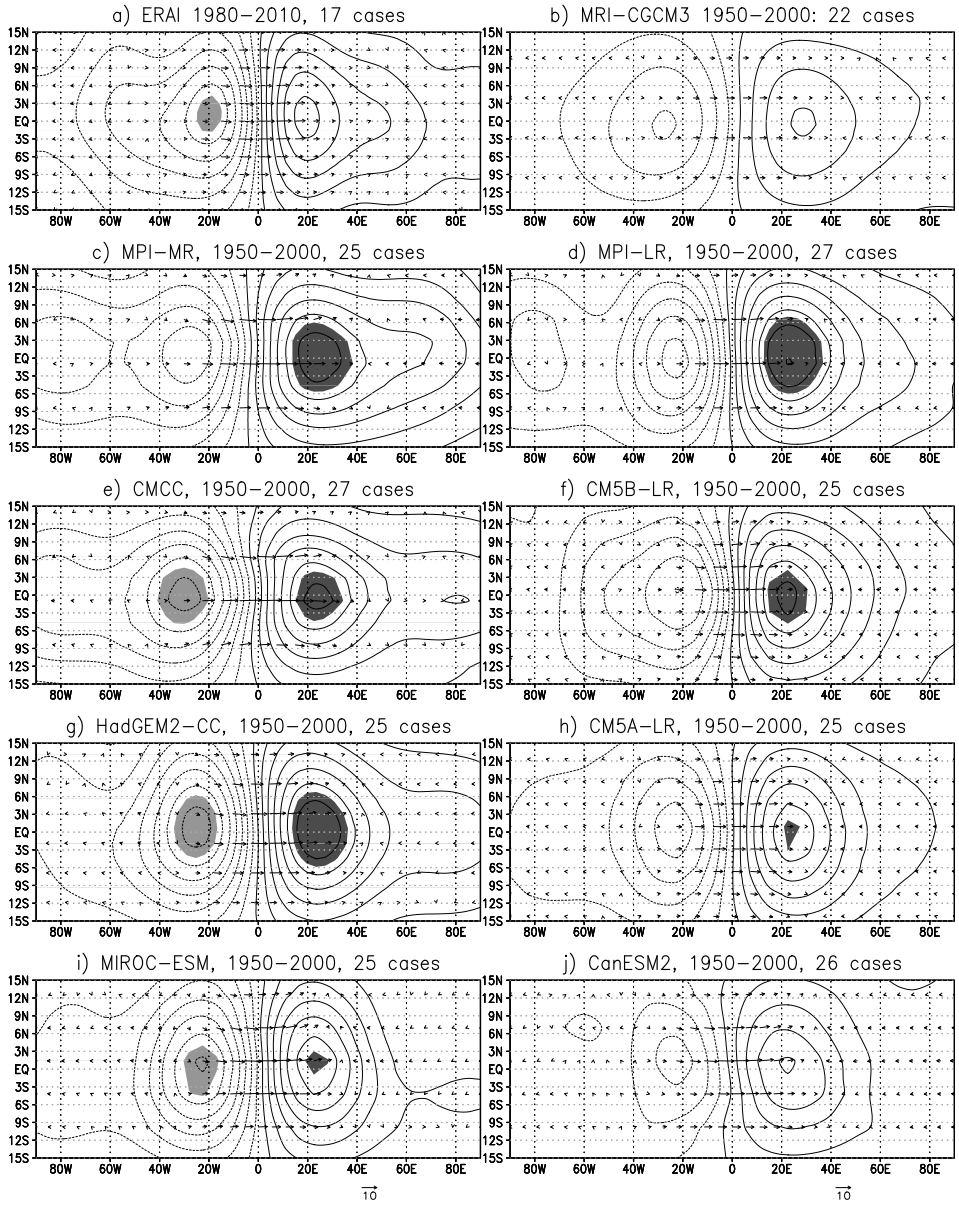

Figure 6. Composite maps of winds and temperature anomalies due to Kelvin waves at 0-day lag and at 50hPa. The contours are for the temperature with contour interval=0.75K and with values below $-3K$ and above $3K$ light shaded and dark shaded respectively. A value of $10m/s$ for the wind arrows is indicated by the arrows below the lower two panels and is identical for all panels.

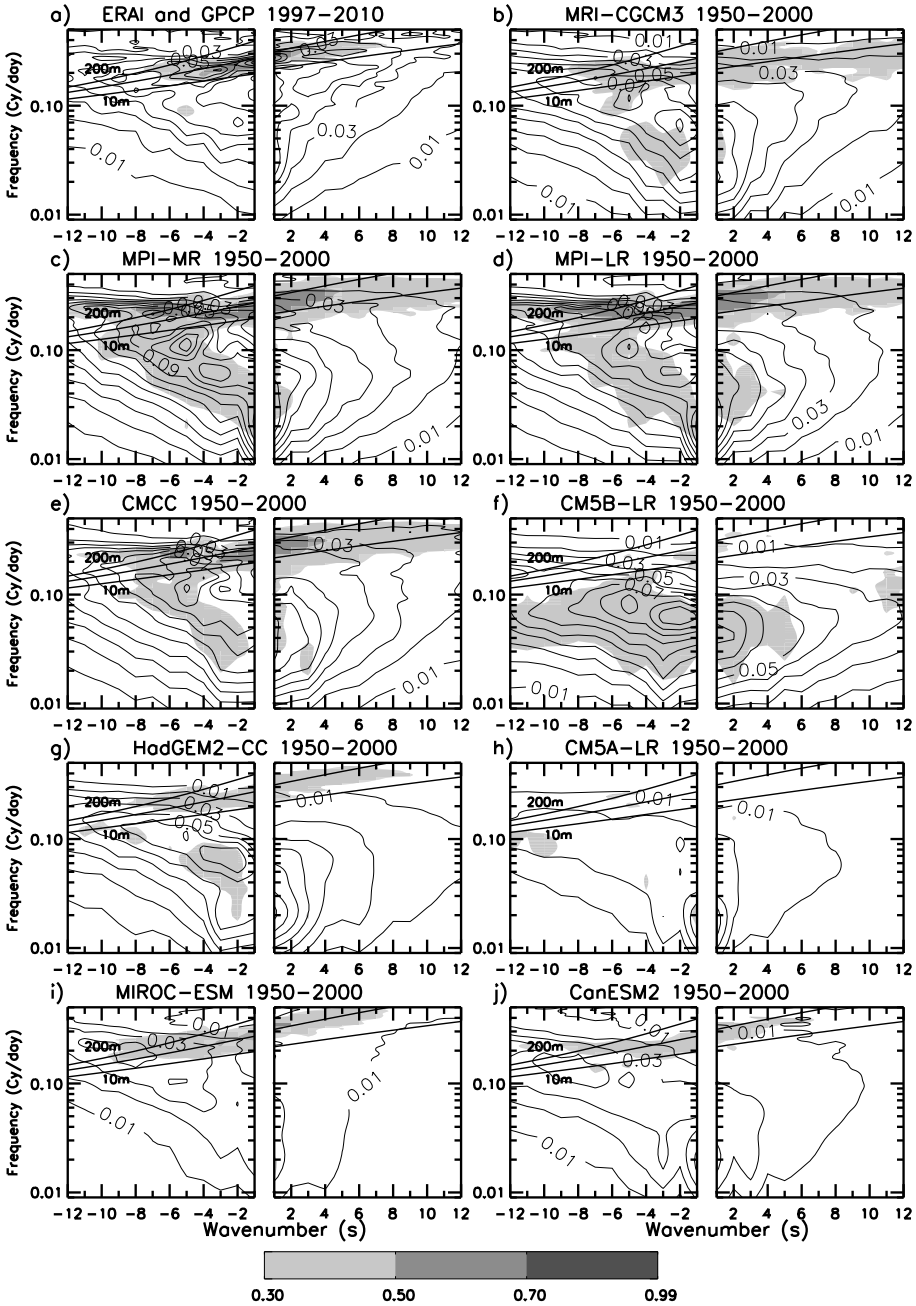

Figure 7. Spectra of anti-symmetric precipitations (contour lines, interval 0.01mm^{2}day^{-3}) and squared coherency with the meridional wind at 850hPa (shading). To build spectra and coherencies, the periodograms and cross-periodograms are evaluated from meridional wind fields averaged over the equatorial band as in Fig. 1. The anti-symmetric precipitation is estimated by multiplying the precipitation field by a sin taper of 20^o width centered at the Equator and then averaged in latitude over (10^{o}S-10^{o}N). In all figures also the dispersion curves are shown for Rossby gravity waves with $h = 10, 40, 200$m.

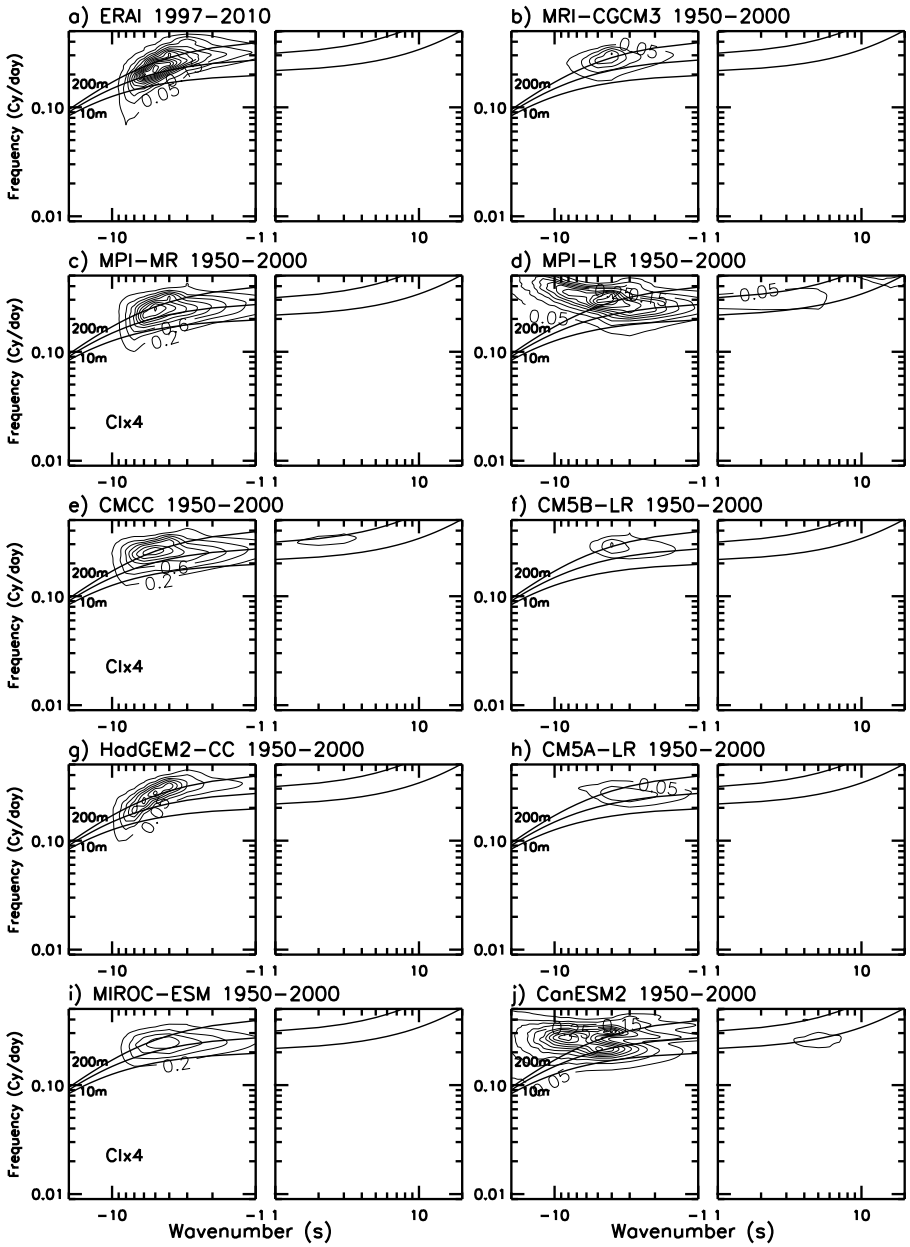

Figure 8. Spectra of the meridional wind at 50hPa and averaged over the equatorial band (contour interval: $0.05 \mathrm{m}^2\mathrm{s}^{-2}\mathrm{day}^{-1}$).

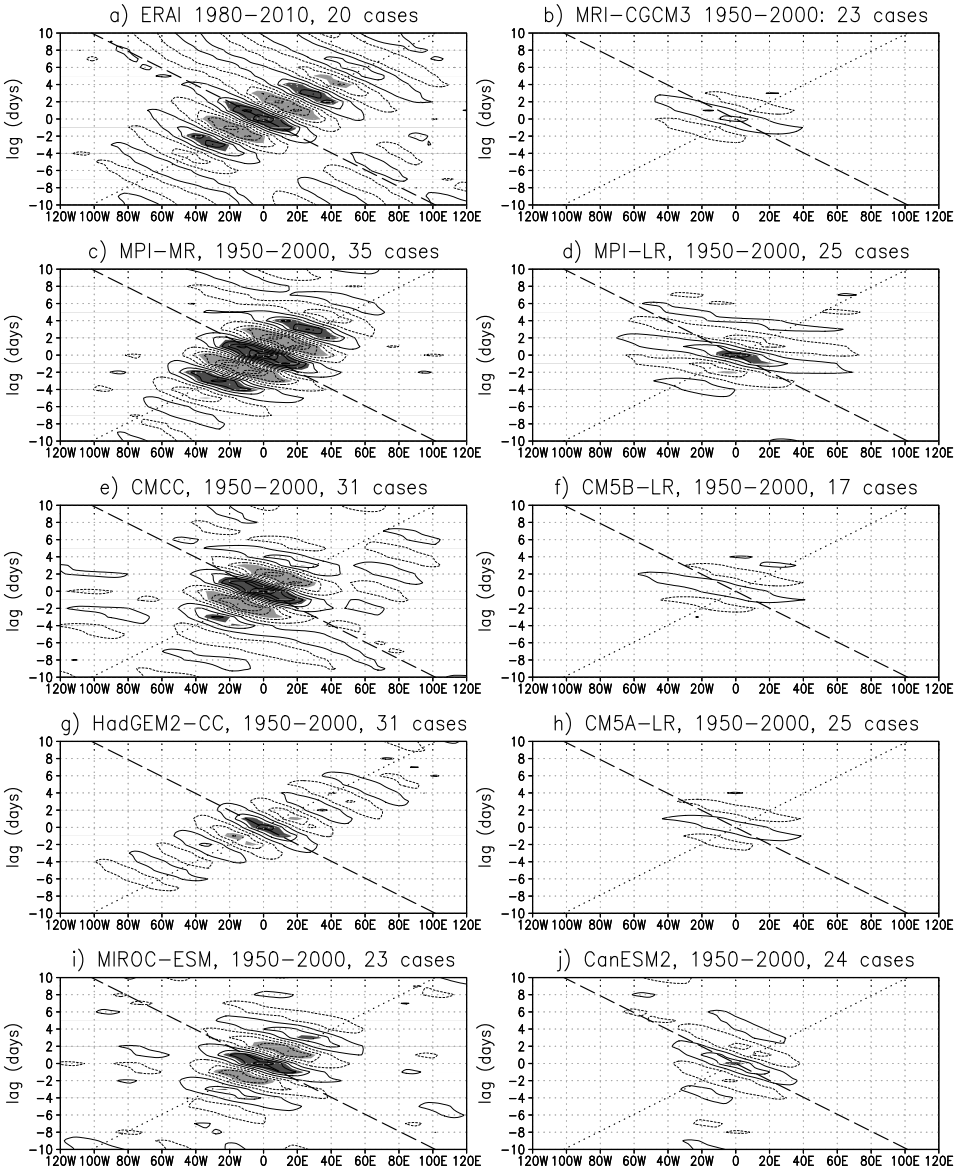

Figure 9. Time evolution of the meridional wind anomaly at the equator due to the passage of Rossby gravity waves at 50hPa, contour interval=1m/s, values below $-2m/s$ and above $2m/s$ are grey shaded and dark shaded respectively. The dotted and dashed lines are for horizontal displacement at the speeds of $\pm 13m/s$ respectively

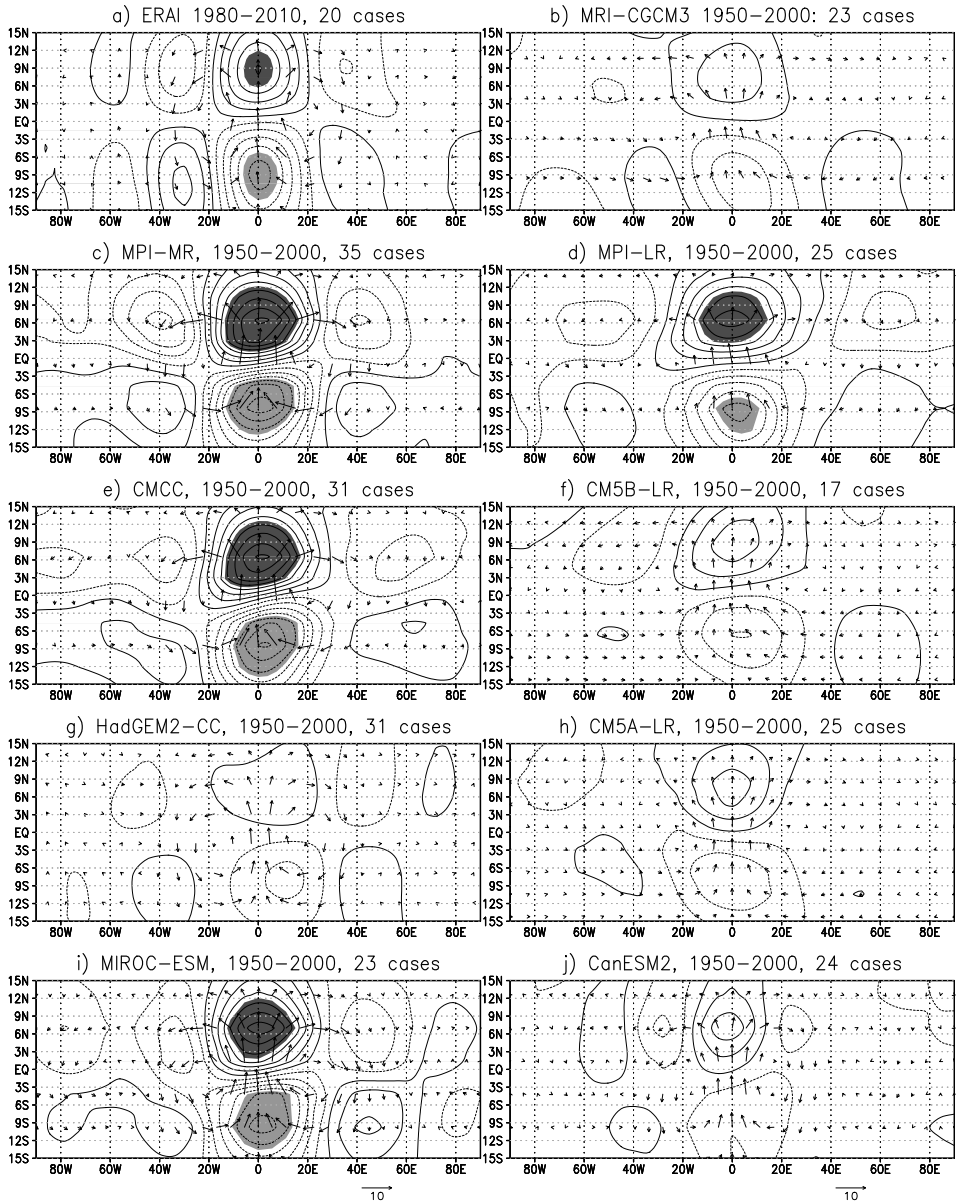

Figure 10. Composite maps of winds and temperature for the Rossby-gravity waves at 0-day lag and at 50hPa. Contour Interval 0.25K, values below -1K and above 1K are grey shaded and dark shaded, respectively. A value of $10m/s$ for the wind arrows is indicated by the arrows below the lower two panels and is identical for all panels.